MAGNETIC RESONANCE IN CHEMISTRY
Magn. Reson. Chem. 2003; **41**: S80–S88
Published online in Wiley InterScience (www.interscience.wiley.com). DOI: 10.1002/mrc.1280

Review

Transverse relaxation–optimized NMR spectroscopy with biomacromolecular structures in solution†

Kurt Wüthrich and Gerhard Wider*

Institut für Molekularbiologie und Biophysik, Eidgenössische Technische Hochschule Zürich, Zürich, Switzerland

1 INTRODUCTION

NMR spectroscopy with biological macromolecules has been limited to relatively small structures, with molecular weights up to about 50 kDa, and the size distribution of the approximately 2500 NMR deposits in the Protein Data Bank peaks near a molecular weight of 10 kDa.[1] In spite of this limitation, NMR is one of the principal experimental techniques in structural biology.[2,3] Nonetheless, the availability of solution NMR techniques for studies of larger structures is of keen interest, in particular for applications in the newly emerging field of structural and functional genomics.[4] With the presently described principles of transverse relaxation-optimized spectroscopy (TROSY) the size limit for molecular structures that are amenable to high resolution NMR studies in solution has been extended severalfold.[5–7] TROSY-based NMR experiments are particularly well suited for applications with proteins and nucleic acids,[8] which are a main focus also in the present article.

2 THE FOUNDATIONS OF TRANSVERSE RELAXATION-OPTIMIZED SPECTROSCOPY (TROSY)

At the high magnetic fields typically used for studies of proteins and nucleic acids, chemical shift anisotropy (CSA) of ^{1}H, ^{15}N and ^{13}C nuclei can be a significant source of transverse relaxation, in addition to the omnipresent relaxation due to dipole–dipole coupling. As a consequence the individual multiplet components in heteronuclear two-spin systems, such as ^{15}N–^{1}H in amide groups and aromatic ^{13}C–^{1}H moieties, may have different transverse relaxation times (Figure 1), and in large structures studied at high magnetic fields these individual relaxation rates are actually largely different.[7] Heteronuclear decoupling, which is routinely applied in conventional NMR spectroscopy,[9] will then lead to a deteriorated averaged signal due to the mixing of the different relaxation rates. In TROSY-type experiments the multiplet structures (Figures 1 and 2) are not decoupled, and only the narrowest, most slowly relaxing line of each multiplet is retained.[10]

2.1 Theory

For a system of two scalar-coupled spin 1/2, I and S, a straightforward description of TROSY can be obtained with the use of single-transition, zero-quantum and double-quantum basis operators.[7] In this basis the individual transverse relaxation rates of all six coherences in a coupled two-spin system (Figure 1) can readily be expressed. Taking only dipole–dipole coupling and CSA relaxation into account, the differential equation (1) describes the time evolution of the system in the slow tumbling limit, where we retain only terms with the spectral density at zero frequency, $J(0)$:

$$\frac{d}{dt}\begin{bmatrix}\langle I_{13}^{\pm}\rangle\\ \langle I_{24}^{\pm}\rangle\\ \langle S_{12}^{\pm}\rangle\\ \langle S_{34}^{\pm}\rangle\\ \langle DQ^{\pm}\rangle\\ \langle ZQ^{\pm}\rangle\end{bmatrix} = -\begin{bmatrix}\pm i\omega_{13}^{I}+R_{13}^{I} & & & & & \\ & \pm i\omega_{24}^{I}+R_{24}^{I} & & 0 & & \\ & & \pm i\omega_{12}^{S}+R_{12}^{S} & & & \\ & & & \pm i\omega_{34}^{S}+R_{34}^{S} & & \\ & 0 & & & \pm i\omega_{14}^{DQ}+R_{14}^{DQ} & \\ & & & & & \pm i\omega_{23}^{ZQ}+R_{23}^{ZQ}\end{bmatrix}\cdot\begin{bmatrix}\langle I_{13}^{\pm}\rangle\\ \langle I_{24}^{\pm}\rangle\\ \langle S_{12}^{\pm}\rangle\\ \langle S_{34}^{\pm}\rangle\\ \langle DQ^{\pm}\rangle\\ \langle ZQ^{\pm}\rangle\end{bmatrix} \quad (1)$$

ω_{ik} are the frequencies of individual transitions in the IS spin system, and R_{ik} are the associated transverse relaxation rates (Figure 1). DQ stands for double-quantum transition, and ZQ for zero-quantum transition. With the assumption that the CSA tensor is axially symmetric, the relaxation rates R_{ik} are

$$R_{13}^{I} = (p^2 + 2f_I p\delta_I + \delta_I^2)\cdot 4J(0) \quad (2a)$$

*Correspondence to: Gerhard Wider, Institut für Molekularbiologie und Biophysik, Eidgenössische Technische Hochschule Zürich, Zürich, Switzerland. E-mail: gsw@mol.biol.ethz.ch
†Reprinted with permission from *Encyclopedia of Nuclear Magnetic Resonance*, volume 9, *Advances in NMR*, D. M. Grant and R. K. Harris (eds), Wiley: Chichester, 2002; 468–477.

Copyright © 2003 John Wiley & Sons, Ltd.

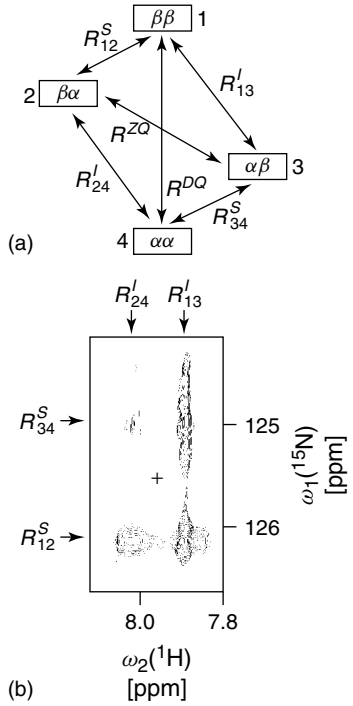

Figure 1. (a) Diagram of the energy levels 1–4 of a system of two scalar-coupled spins 1/2, *I* and *S*, with indication of the transverse relaxation rates, *R*, of the individual transitions. The abbreviations ZQ and DQ stand for zero-quantum and double-quantum transitions. (b) Cross-peak of a backbone amide moiety from a two-dimensional [^{15}N,^{1}H]-HSQC spectrum of uniformly ^{2}H,^{13}C,^{15}N-labeled 7,8-dihydroneopterin aldolase (DHNA) from *Staphylococcus aureus* measured without ^{1}H and ^{15}N decoupling. DHNA is a homo-octameric protein of molecular weight 110 kDa.[44] The NMR sample contained 0.4 mM DHNA octamer, solvent 90% H_2O/10% D_2O, pH = 6.5, $T = 20\,^\circ$C, ^{1}H frequency = 750 MHz. The relaxation rates that are effective for the individual multiplet components are indicated at the top and on the left. The cross marks the center of the multiplet, i.e., the position of the single-component cross peak in a ^{1}H and ^{15}N broadband decoupled spectrum.

$$R^I_{24} = (p^2 - 2f_I p\delta_I + \delta_I^2)\cdot 4J(0) \tag{2b}$$

$$R^S_{12} = (p^2 + 2f_S p\delta_S + \delta_S^2)\cdot 4J(0) \tag{2c}$$

$$R^S_{34} = (p^2 - 2f_S p\delta_S + \delta_S^2)\cdot 4J(0) \tag{2d}$$

$$R^{DQ} = (\delta_I^2 + 2f_c\delta_I\delta_S + \delta_S^2)\cdot 4J(0) \tag{2e}$$

$$R^{ZQ} = (\delta_I^2 - 2f_c\delta_I\delta_S + \delta_S^2)\cdot 4J(0) \tag{2f}$$

In equation (2), p is the dipolar interaction energy,

$$p = \frac{\mu_0 h\gamma_I\gamma_s}{16\pi^2\sqrt{2}r_{IS}^3} \tag{3}$$

δ_s the ^{15}N-chemical shift anisotropy interaction,

$$\delta_S = \frac{\gamma_S B_o \Delta\sigma_S}{3\sqrt{2}} \tag{4}$$

and δ_I the ^{1}H-chemical shift anisotropy interaction,

$$\delta_I = \frac{\gamma_I B_o \Delta\sigma_I}{3\sqrt{2}} \tag{5}$$

The factor f_i accounts for the angular dependence of cross correlated relaxation effects, with

$$f_i = \frac{3\cos^2\Theta_i - 1}{2} \tag{6}$$

For dipole–dipole coupling/CSA cross correlation, Θ_i is the angle between the principal axis of the axially symmetric CSA tensor and the chemical bond linking the spins *I* and *S* (in equation (6), $i = S$ or I; see equation (2)). For CSA/CSA cross correlation, Θ_i is the angle between the two CSA tensor principal axes (in equation (6), $i = c$; see equation (2)). For isotropically tumbling spherical structures the spectral density function at zero frequency is given by

$$J(0) = \frac{2\tau_c}{5} \tag{7}$$

where τ_c is the rotational correlation time of the molecule.

Equation (2) shows that for non-vanishing CSA values the single-quantum transitions, which represent the two fine structure components of the *I* and *S* doublets, have different relaxation rates. Since p is field-independent and the CSA interaction increases in proportion to the field strength, there is a 'magic field' for one of the doublet components where its relaxation rate will be near zero, whereas the other component deteriorates due to rapid relaxation. For ^{15}N in peptide ^{15}N–^{1}H groups one approaches this situation at the highest presently available ^{1}H frequencies of 900 MHz, and for the amide proton a minimal transverse relaxation rate is expected near 1000 MHz.[5,7] For the zero-quantum and double-quantum transitions a different mechanism is responsible for the different relaxation rates of the individual fine structure components, i.e., cross correlation between the CSAs of the *I* and *S* spins [equations (2e) and (2f)]. This effect has been exploited for relaxation optimization in the three-dimensional NOESY-[^{1}H,^{15}N,^{1}H]-ZQ-TROSY experiment.[11]

For the practice of TROSY-NMR, one should keep in mind that some leakage is anticipated even for the 'magic field condition' of complete quenching of the transverse relaxation for an isolated two-spin system. Most important, relaxation of the spins in ^{15}N–^{1}H moieties by dipole–dipole coupling with 'remote' protons, i.e., all protons outside of the ^{15}N–^{1}H group, is the same for conventional NMR and for TROSY. This effect is minimized in uniformly deuterated proteins, where remote couplings are limited to other amide protons. For ^{15}N–^{1}H groups the relative contributions from remote dipolar couplings to the overall transverse relaxation rates of the two spins are widely different. ^{15}N relaxation is dominated by the CSA of ^{15}N and the dipole–dipole interactions with the directly attached proton even in protonated proteins, but $^1H^N$ transverse relaxation is significantly enhanced by dipole–dipole interactions with remote protons, H_k, at distances r_k from the amide proton, as given by

$$R_L = \sum_{k=1}^{n} 5p_k^2 \cdot J(0) \tag{8}$$

with

$$p_k = \frac{\mu_0 h\gamma_H^2}{16\pi^2\sqrt{2}r_k^3} \tag{9}$$

Copyright © 2003 John Wiley & Sons, Ltd.

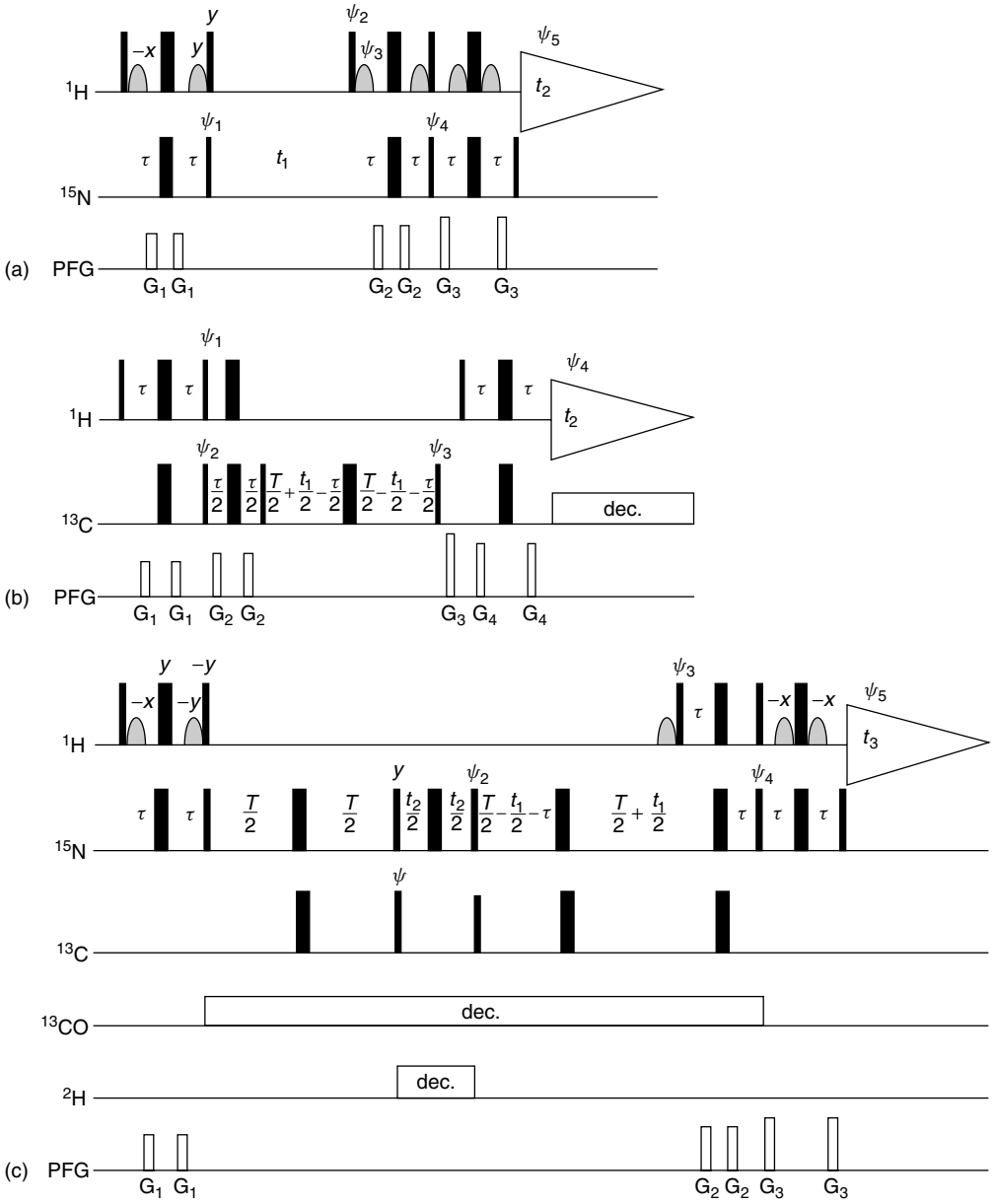

Figure 2. Experimental schemes for three TROSY-type NMR experiments: (a) [^{15}N,^{1}H]-TROSY correlation experiment; (b) ct-[^{13}C,^{1}H]-TROSY correlation experiment; (c) [^{15}N,^{1}H]-TROSY-HNCA triple resonance experiment. On the lines marked ^{1}H,^{13}C and ^{15}N, narrow and wide bars stand for non-selective 90° and 180° radio-frequency pulses, respectively. In (a) and (c), water saturation is minimized by keeping the water magnetization along the $+z$-axis during the entire experiment, using the water-selective 90° rf-pulses indicated by curved shapes on the line ^{1}H.[9] The phases of the pulses are set to x unless indicated otherwise above the pulse. In (a) and (c), the ^{15}N evolution period is marked t_1, in (b) the ^{13}C evolution period is t_1, in (c) the ^{13}C evolution period is t_2, and in all experiments the ^{1}H detection period is represented by a triangle. The line marked PFG indicates the pulsed magnetic field gradients applied along the z-axis. On the lines ^{13}C in (b), and ^{13}CO and ^{2}H in (c), the horizontal bars marked 'dec.' indicate periods of broadband decoupling. In (a), the time period τ is set to 2.7 ms; the phases for the pulses are $\psi_1 = \{y, -x\}$, $\psi_2 = \{-y\}$, $\psi_3 = \{y\}$, $\psi_4 = \{-y\}$, ψ_5(receiver) $= \{y, -x\}$, and a complex interferogram is obtained by recording a second FID for each t_1 delay, with $\psi_1 = \{y, x\}$, $\psi_2 = \{y\}$, $\psi_3 = \{-y\}$, $\psi_4 = \{y\}$. In (b), $\tau = 1.6$ ms, $T = 17.6$ ms; the phases for the pulses are $\psi_1 = \{-y\}$, $\psi_2 = \{\pi/4, 5\pi/4\}$, $\psi_3 = \{x, -x, -x, -x\}$, $\psi_4 = \{x, -x, -x, x\}$. A phase-sensitive spectrum in the t_1 dimension is obtained as described in Ref. 12 In (c), $\tau = 2.7$ ms, $T = 22$ ms; the phases for the pulses are $\psi_1 = \{x, x, -x, -x\}$, $\psi_2 = \{y, -y, -x, x\}$, $\psi_3 = \{y\}$; $\psi_4 = \{y\}$, $\psi_5 = \{y, -y, -x, x, -y, y, x, -x\}$. A phase-sensitive spectrum in the indirect dimensions is obtained as described in Ref. 45.

The overall relaxation rates for the individual multiplet components are obtained by addition of R_L (equation (8)) to one of the rates given in equations (2a), (2b), (2e) or (2f).[7] In addition to remote dipolar couplings, deviations of the CSA tensors from axial symmetry and variable spatial orientations of the CSA tensors relative to the molecular structure may prevent the ideal 'magic field condition' for a given two-spin moiety, and cause the individual ^{15}N–^{1}H groups in a protein to get closest to the 'magic field condition' at slightly different polarizing magnetic fields B_o.

Copyright © 2003 John Wiley & Sons, Ltd.

2.2 Experimental Implementation of TROSY

Essential features of successful TROSY implementations are that the multiplet fine structure of the *IS* moieties is not decoupled, and that the desired slowly relaxing component, i.e., the one with the relaxation rates R_{13}^{I} and R_{12}^{S} [see Figure 1 and equation (2); note in equation (2) that for $I = {}^{1}H$ and $S = {}^{15}N$, p is a negative value], can be selectively detected with high sensitivity. A simple scheme for the application of the TROSY principle is the single-quantum $^{15}N-^{1}H$ correlation experiment (Figure 2a). For brevity we refer to this experiment as two-dimensional [^{15}N,^{1}H]-TROSY.[12] There is no heteronuclear decoupling in the scheme of Figure 2(a), so that the transitions with different relaxation rates (Figure 1) are not mixed. The phase cycling, the pulsed field gradients and the additional pulse on ^{15}N immediately before acquisition ensure that only the most slow relaxing transition in a $^{15}N-^{1}H$ moiety is retained. The effects on the appearance of the spectrum are illustrated in Figure 3.[10] In the conventional two-dimensional [^{15}N,^{1}H]-COSY experiment,[13] decoupling of ^{15}N and ^{1}H during the evolution and detection periods, respectively, leads to observation of a single correlation peak per $^{15}N-^{1}H$ moiety (Figure 3a). If the same spectrum is recorded without decoupling, a four-line fine structure is observed where the individual components have largely different linewidths (Figure 3b). Only the narrowest one of these four lines is observed in [^{15}N,^{1}H]-TROSY (Figure 3c).

The anticipated sensitivity loss due to retaining only one of the four multiplet components in [^{15}N,^{1}H]-TROSY can be largely made up by the use of new polarization transfer elements. In the scheme of Figure 2(a), the ST2-PT element is used before data acquisition, which retains 50% rather than only 25% of the original proton polarization.[12] Furthermore, in the absence of decoupling the steady-state heteronuclear magnetization can be used in addition to the proton polarization.[12,14] Overall, when working with structure sizes above 20 kDa, a superior ratio of peak height to noise is thus typically achieved with TROSY when compared with the corresponding conventional experiments (see Section 3).

3 TROSY IN NMR EXPERIMENTS WITH BIOLOGICAL MACROMOLECULES

3.1 TROSY in $^{15}N-^{1}H$ Correlation Experiments

The Figure 4(a) shows a two-dimensional [^{15}N,^{1}H]-TROSY spectrum measured with the experimental scheme of Figure 2(a) for the 110 kDa homo-octameric protein DHNA (see legend to Figure 1). The gain in spectral resolution is readily apparent from comparison with the corresponding conventional two-dimensional [^{15}N,^{1}H]-COSY experiment (Figure 4b). Two-dimensional [^{15}N,^{1}H]-TROSY experiments can provide a 'fingerprint' for proteins in severalfold larger structures than with conventional NMR.[15] The $^{15}N-^{1}H$ fingerprint is highly sensitive to changes in the protein environment and thus presents a many-parameter NMR probe for studies of intermolecular interactions. For example, chemical shift mapping of the amide groups is used in SAR by NMR (SAR stands for 'structure-activity relationship'),[16] which is a screening method for high-affinity ligands of macromolecular receptors. With the use of two-dimensional [^{15}N,^{1}H]-TROSY this approach will now be applicable for much bigger receptor molecules, with molecular weights of the order of 100 kDa. Similarly, comparison of the fingerprints of individual proteins in the free state and incorporated in supramolecular structures enables the mapping of intermolecular contacts with these proteins in the higher-order structures.[17] The introduction of the TROSY technique thus opens a wide range of new applications for solution NMR, in particular also in the newly emerging field of functional genomics.

3.2 TROSY in $^{13}C-^{1}H$ Correlation Experiments

The TROSY principle is not limited to $^{15}N-^{1}H$ groups, but may be effective in a variety of multi-spin systems with cross correlated relaxation effects. As an illustration, we present here a constant-time $^{13}C-^{1}H$ correlation experiment with aromatic rings of a protein, which can also be applied with ring $^{13}C-^{1}H$ moieties of DNA and RNA. The spectrum of Figure 5 was obtained with the experiment of Figure 2(b). Since the aromatic protons have very small CSA, TROSY is used only in the ^{13}C dimension and the experiment includes decoupling during acquisition. In this constant-time experiment, TROSY does not affect the line shape but improves the sensitivity.[14] Figure 5 shows that a four- to ten-fold signal enhancement was achieved for individual resonances of the aromatic rings in an experiment with a protein of molecular weight 16 kDa, and similar signal enhancements have been obtained for RNA and DNA molecules.[18,19] For aromatic $^{13}C-^{1}H$ groups the 'magic field' is approached near a ^{1}H frequency of 600 MHz, and applications of [^{13}C, ^{1}H]-TROSY are of interest for ^{13}C-labeled proteins and nucleic acids of all sizes.

3.3 TROSY for Observation of Scalar Couplings Across Hydrogen Bonds

Hydrogen bonds are key elements for the architecture of three-dimensional structures of proteins and nucleic acids as well as for intermolecular recognition. Their presence in biological macromolecules is usually only indirectly inferred from experimental data.[20] The improved spectral resolution achieved with TROSY now enables observation of scalar couplings across hydrogen bonds in nucleic acids as well as in proteins.[21–24] As an illustration, Figure 6 shows a [^{15}N,^{1}H]- TROSY correlation experiment recorded with high resolution along the ω_1(^{15}N) dimension for the determination of scalar couplings across hydrogen bonds in Watson-Crick base pairs. Such data can be obtained using transverse relaxation optimization during a long ^{15}N evolution period, thereby accepting low sensitivity in order to achieve high resolution along the 'indirect' heavy-atom frequency axis. The $^{h2}J_{NN}$ couplings seen in Figure 6 are in the range 3–7 Hz; for smaller couplings across hydrogen bonds, more refined observation schemes are available.[24]

3.4 TROSY in Triple Resonance Experiments for NMR Assignments in Large Structures

The assignment of the chemical shifts to individual nuclei is indispensable as a basis for detailed studies of either

Copyright © 2003 John Wiley & Sons, Ltd.

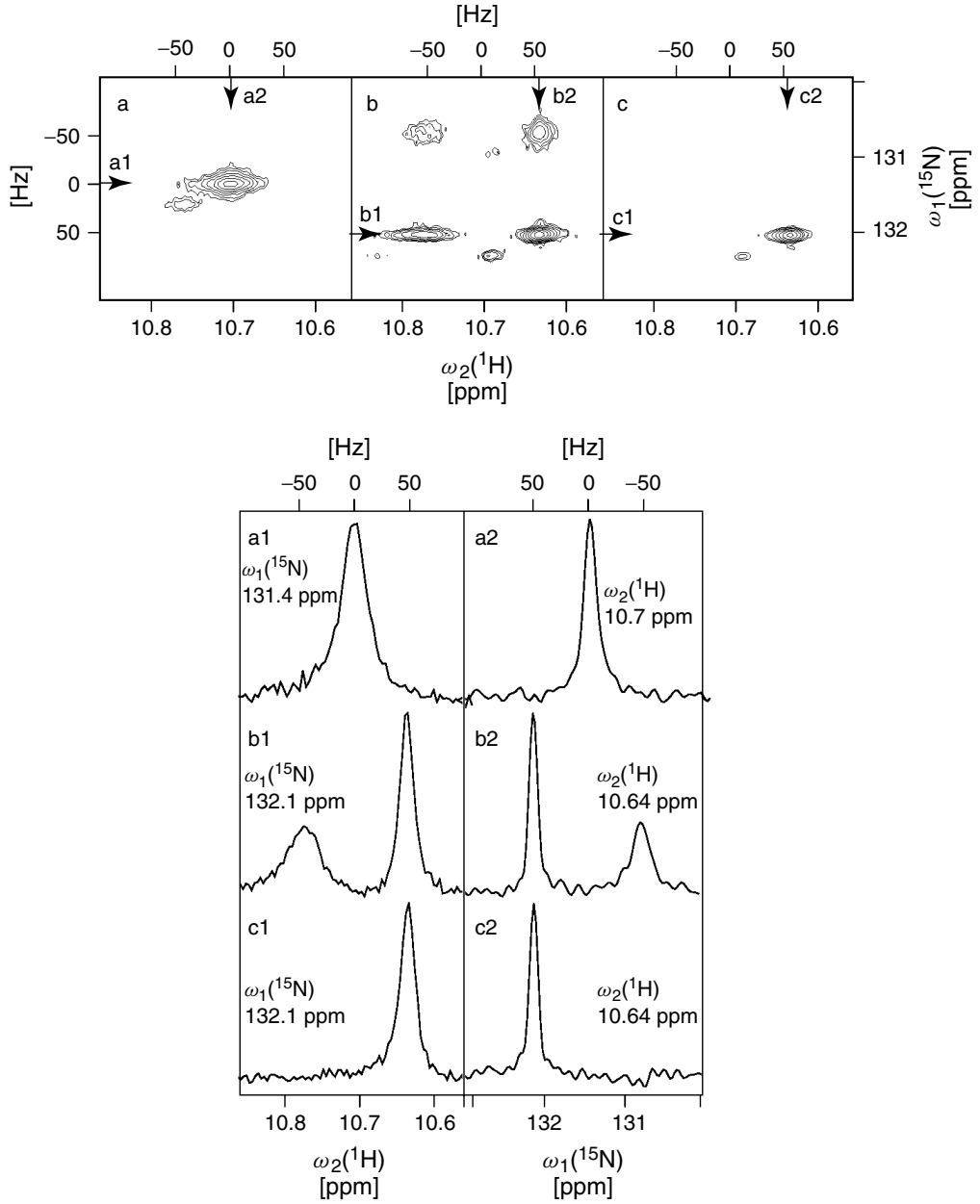

Figure 3. Contour plots and cross sections of a backbone amide ^{15}N–^1H correlation cross peak (see also Figure 1) obtained from three different types of ^{15}N–^1H correlation experiments. The data was recorded with the uniformly ^{15}N-labeled protein *fushi tarazu* homeodomain in an 18 kDa complex with unlabeled DNA, solvent 95% H_2O/5% D_2O, $T = 4\,^\circ C$, pH = 6.0, ^1H frequency = 750 MHz. (a) Conventional broad-band-decoupled [^{15}N,^1H]-COSY spectrum. (b) Same as (a) without decoupling during the evolution and detection periods. (c) [^{15}N,^1H]-TROSY recorded with the scheme of Figure 2(a). The arrows in the contour plots indicate the positions of the cross sections displayed in the bottom panels. The figure visualizes why corresponding peaks in COSY and TROSY spectra are displaced by 0.5 $^1J_{IS}$ (ca. 45 Hz for ^{15}N–^1H) along both frequency axes. (Adapted from Ref. 10).

molecular structure or intermolecular interactions, and most of the information contained in NMR spectra can only be extracted and exploited on the basis of individual resonance assignments.[15] Once high-quality spectra became available with TROSY, it was therefore of keen interest to develop NMR techniques that can provide resonance assignments for large proteins. Both, assignment by sequential NOEs with ^2H,^{15}N- or ^{15}N-labeled proteins and by triple resonance experiments with ^2H,^{13}C,^{15}N- or ^{13}C,^{15}N-labeled proteins appear to be amenable to this task,[9,15,25] but most of the work so far was done on the adaptation of triple resonance experiments for assignments in large molecules. In these experiments magnetization is transferred between $^1H^N$,^{15}N and ^{13}C. Without the use of TROSY they have been routinely applied with structures of size 15 to about 30 kDa.

In triple-resonance experiments with large proteins the implementation of TROSY prevents fast transverse relaxation of ^{15}N during the extended time periods with transverse ^{15}N magnetization that are needed for polarization transfers and ^{15}N evolution, and reduces the transverse ^1H relaxation rate during the acquisition of the amide proton signal.[26] This is illustrated here with the HNCA experiment. The

Copyright © 2003 John Wiley & Sons, Ltd.

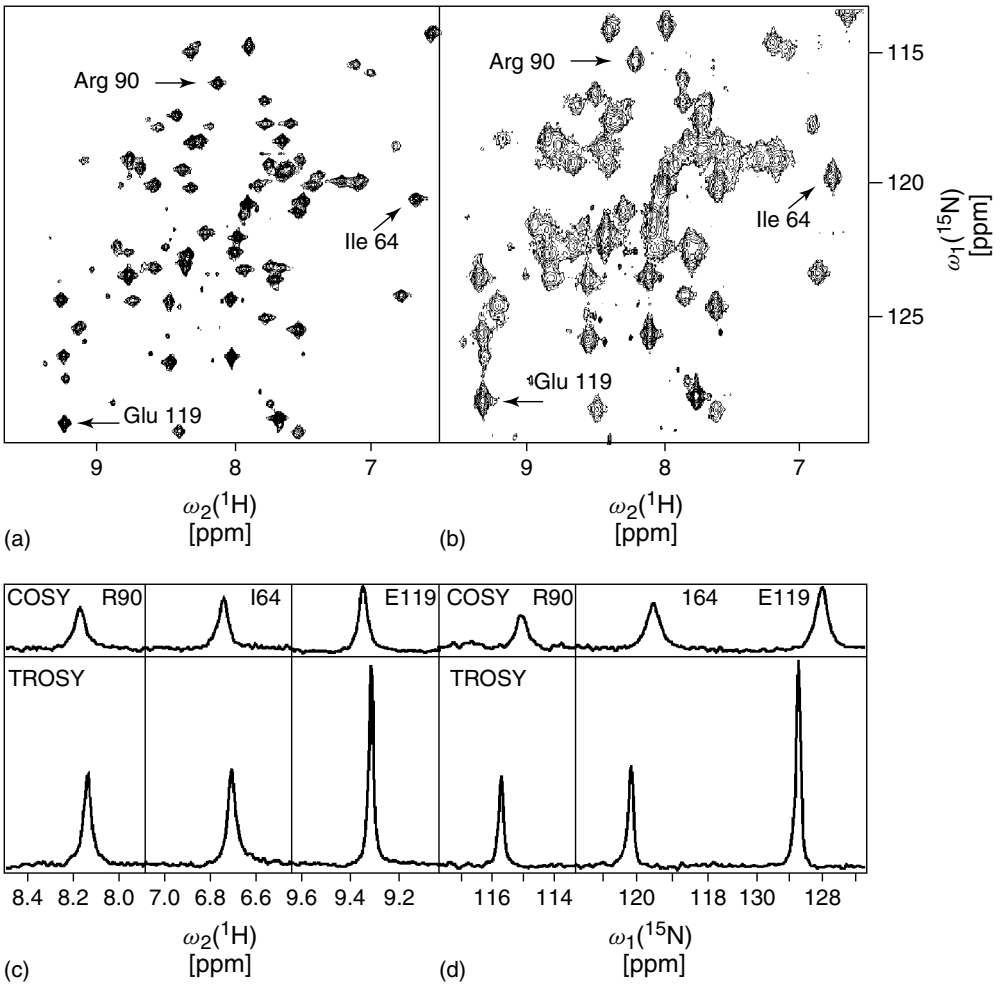

Figure 4. Comparison of conventional and TROSY-type $^{15}N-^{1}H$ correlation spectra recorded with the 110 kDa protein DHNA (same sample as in Figure 1). (a) Contour plot of [^{15}N,^{1}H]-TROSY; (b) Contour plot of single-quantum [^{15}N,^{1}H]-COSY; (c) and (d) Cross sections along $\omega_2(^1H)$ and $\omega_1(^{15}N)$, respectively, through the three peaks identified in the contour plots with an arrow, the amino acid symbol and the sequence position. In the cross sections one readily observes that corresponding peaks in [^{15}N,^{1}H]-COSY and [^{15}N,^{1}H]-TROSY spectra are displaced along both frequency axes by about 45 Hz (see Figure 3).

magnetization transfer pathway is indicated in Figure 7(a), and an experimental scheme is shown in Figure 2(c). Since the triple resonance experiments of interest usually contain a 'constant-time evolution period' for ^{15}N,[9,27] implementation of TROSY does not affect the ^{15}N line shape but yields important gains in sensitivity, which are dependent on the size of the molecule studied. The use of TROSY in triple resonance experiments has enabled backbone assignments for proteins in large structures, such as the 110 kDa ^{2}H,^{13}C,^{15}N-labeled octameric protein DHNA.[28] For this structure, TROSY yielded 20- to 50-fold signal enhancements for individual residues in the structured segments of the polypeptide chain, and only the highly flexible C-terminal residue Lys 121 gave comparable results with and without TROSY (Figure 7).

With TROSY-type triple resonance experiments, sequential assignments can now routinely be obtained for proteins in structures with molecular weights of 100 000 and beyond. On top of this 'basic TROSY effect' the modified triple resonance experiments can be further optimized, for example, for improved spectral resolution through the use of ^{13}C constant-time evolution,[29] or for further optimization of the sensitivity with the introduction of one of a variety of sensitivity enhancement schemes, which have in part also been used for [^{15}N,^{1}H]-TROSY and [^{13}C,^{1}H]-TROSY.[7]

4 NEW STABLE ISOTOPE LABELING STRATEGIES FOR TROSY NMR WITH LARGE STRUCTURES

With TROSY enabling the recording of high-quality solution NMR spectra of large structures, one can anticipate being faced with highly complex NMR spectra. Actually, many large systems give spectra of manageable complexity. Examples are uniformly labeled oligomeric proteins with high internal symmetry, and isotope-labeled proteins in complexes with unlabeled nucleic acids or unlabeled lipids and detergents. In contrast, uniformly labeled proteins without internal symmetry show increasing complexity of the NMR spectrum with increasing size. As a response to this challenge there are now already new biochemical approaches available for reducing the spectral complexity to

Copyright © 2003 John Wiley & Sons, Ltd.

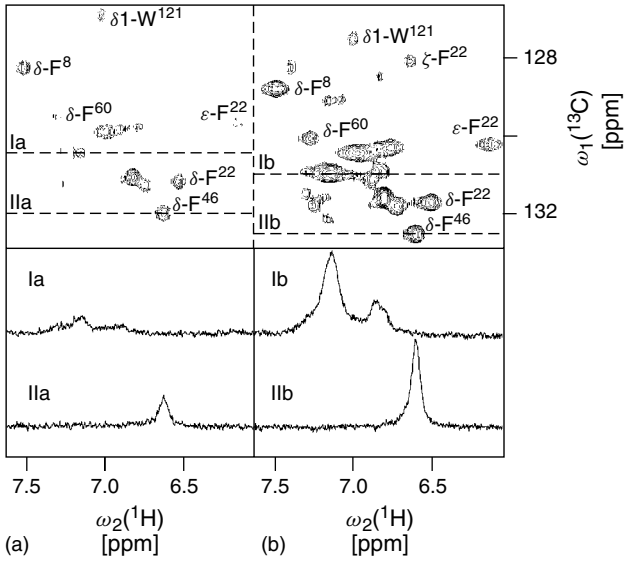

Figure 5. Comparison of two different $^{1}H-^{13}C$ correlation experiments recorded with the uniformly ^{13}C-labeled 16 kDa protein cyclophilin A. In the NMR sample the protein concentration was 1 mM, solvent D_2O, pD = 6.5, $T = 10\,^{\circ}C$, ^{1}H frequency 750 MHz. The spectral region shown contains aromatic resonances. (a) Two-dimensional ct-[^{13}C,^{1}H]-COSY; (b) Two-dimensional ct-[^{13}C,^{1}H]-TROSY, recorded using the pulse scheme of Figure 2(b). Corresponding peak positions in the spectra (a) and (b) differ by about 80 Hz along $\omega_1(^{13}C)$, as indicated by the horizontal broken lines, which also identify the locations of the cross sections along ω_2 that are shown in the bottom panels. The assignments of selected cross-peaks are indicated. (Adapted from Ref. 14).

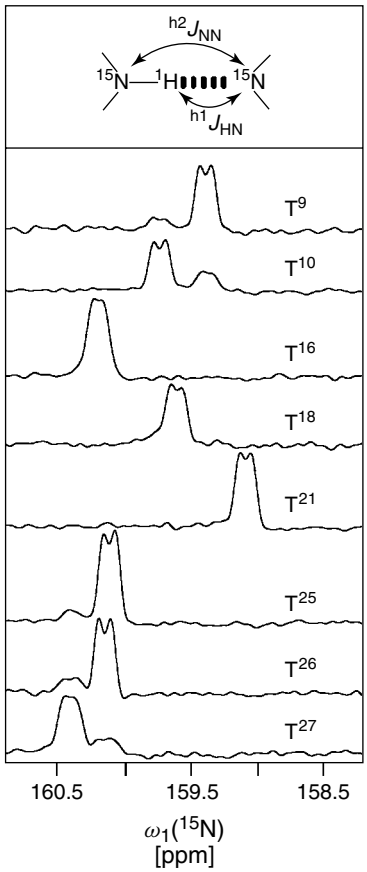

Figure 6. NMR observation of scalar $^{15}N-^{15}N$ couplings across hydrogen bonds in DNA. The definitions of the scalar couplings $^{h2}J_{NN}$ and $^{h1}J_{HN}$ in Watson-Crick base pairs are shown at the top. Cross sections were taken along the $\omega_1(^{15}N)$ dimension through the individual cross peaks of the thymine imino $^{15}N-^{1}H$ moieties in a [^{15}N,^{1}H]-TROSY spectrum of a uniformly ^{13}C,^{15}N-labeled 14-base pair DNA duplex. The splitting of the resonance lines manifests scalar couplings $^{h2}J_{NN}$ of about 6 Hz across the Watson-Crick hydrogen bonds. The nucleotides are numbered in the 5′-to-3′ direction for both strands. (Adapted from Ref. 22).

a manageable level even for large proteins, using segmental isotope labeling.[30–33]

Segmental isotope labeling for protein NMR has been achieved using either transplicing or chemical ligation to assemble proteins from two or more independently generated polypeptide fragments, which are separately produced in bacteria and can thus be obtained with and without isotope labeling. The solution structure of the labeled domain can then be studied by NMR without interference from NMR lines originating from the other domains. By repetition of the NMR experiments using different protein preparations with isotope labeling of different individual domains, the intact protein can become accessible for detailed studies by TROSY-NMR, although it would, because of its large size produce overcrowded NMR spectra if uniform isotope labeling were used.

5 COMBINING TROSY WITH CROSS CORRELATED RELAXATION-INDUCED POLARIZATION TRANSFER FOR STUDIES OF VERY LARGE STRUCTURES

In the common heteronuclear NMR experiments, magnetization is transferred between the different types of nuclei via scalar spin–spin couplings, using INEPT transfers.[9,34] With TROSY being applied only during the evolution and detection periods (Figure 2), rapid transverse relaxation during the INEPT transfers becomes a limiting factor for structures with molecular weights above approximately 100–150 kDa. Cross correlated relaxation-enhanced polarization transfer (CRINEPT) overcomes this limitation by combining INEPT with cross-correlated relaxation-induced polarization transfer (CRIPT).[35,36] The transfer efficiency of CRIPT increases proportional to the size of the molecule, so that it becomes a highly efficient transfer mechanism for structure sizes above 200 kDa in aqueous solution. Compared to combining INEPT with the use of TROSY during the evolution and acquisition periods (Figure 2), substitution of INEPT by CRINEPT can thus yield a further significant gain in sensitivity when studying very large structures. In addition to the improved transfer efficiency, the combination of TROSY and CRINEPT results in an experiment with transverse relaxation optimization throughout the entire pulse sequence. In practice, CRINEPT has so far mainly been used

Copyright © 2003 John Wiley & Sons, Ltd.

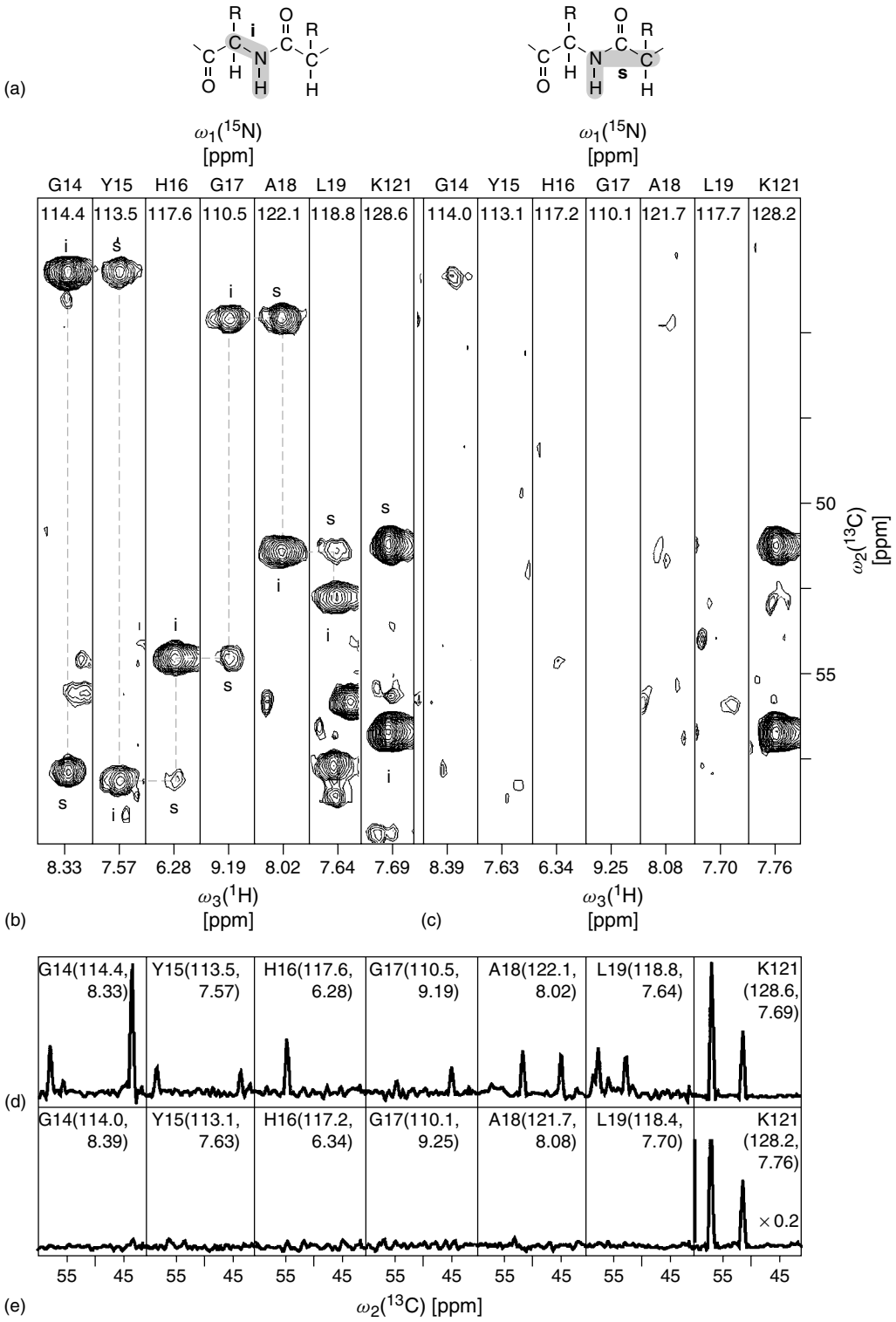

Figure 7. Impact of TROSY on the sequential resonance assignment of the polypeptide backbone in the 110 kDa protein DHNA (same sample as in Figure 1) using the HNCA triple resonance experiment of Figure 2(c). (a) The HNCA experiment correlates the ^{1}H and ^{15}N chemical shifts of a given amide ^{15}N–^{1}H group with the $^{13}C^{\alpha}$ chemical shifts of the same residue, i, and the preceding residue, s, as indicated here by gray shading of the intraresidual and sequential transfer pathways. (b) and (d) Three-dimensional [^{15}N,^{1}H]-TROSY-HNCA spectrum.[46] (c) and (e) Conventional three-dimensional HNCA spectrum. (b) and (c) show strips taken along the $\omega_2(^{13}C)$ dimension at the ^{1}H and ^{15}N resonance frequencies of the residue indicated at the top of the strip. The width of the strips along the ^{1}H-dimension is 130 Hz. (d) and (e) are one-dimensional cross sections along the $\omega_2(^{13}C)$ axis through the peaks in these strips. The dotted line in (b) indicates the sequential assignment pathway for the polypeptide segment 14–19, where the intraresidual and sequential cross peaks are identified with 'i' and 's', respectively (see (a)). The highly flexible C-terminal Lys 121 is the only residue that was observed in both spectra, and it is added here as an internal reference for this experiment (see text). (Adapted from Ref. 28).

Copyright © 2003 John Wiley & Sons, Ltd.

in $^{15}N-^{1}H$-correlation experiments,[8] and high quality fingerprints have been recorded for structures with molecular weights up to 900 kDa.

6 CONCLUSIONS AND OUTLOOK

The most immediate applications of the potentialities of TROSY and CRINEPT are based on observing fingerprints of proteins in $^{15}N-^{1}H$-correlation spectra recorded for structures with mass up to 100 kDa and beyond (Figure 4), for which sequence-specific NMR assignments can be obtained (Figure 7). Practical use for studies of intermolecular interactions in supramolecular assemblies has been described,[17,37] and the way is open for acquiring structure–activity relationship data with large receptor molecules.[38] TROSY-based NOESY experiments for the collection of structural constraints should enable three-dimensional solution structure determination of proteins larger than 50 kDa,[11,39,40] if segmental labeling is also applied. An exciting immediate prospect are structure determination and further physical-chemical and functional characterization of small membrane proteins reconstituted in water-soluble detergent or lipid micelles, which may then have overall molecular weights of the order 100 kDa.[41–43] Further exploration of the potentialities of TROSY and CRINEPT will be supported by future refinement of isotope labeling techniques for proteins and nucleic acids, the use of spectrometers operating at 900 MHz and beyond, and other advances in NMR techniques.[5]

7 REFERENCES

1. P. Güntert, *Q. Rev. Biophys.*, 1998, **31**, 145.
2. K. Wüthrich, *Acta Cryst. D*, 1995, **51**, 249.
3. G. Wider, *BioTechniques*, 2000, **29**, 1278.
4. T. Smith ed, Structural Genomics, *Nature Struct. Biol.*, 2000, **7**, 927.
5. K. Wüthrich, *Nature Struct. Biol.*, 1998, **5**, 492.
6. G. Wider and K. Wüthrich, *Curr. Opin. Struct. Biol.*, 1999, **9**, 594.
7. K. Pervushin, *Q. Rev. Biophys.*, 2000, **33**, 161.
8. R. Riek, K. Pervushin, and K. Wüthrich, *Trends Biochem. Sci.*, 2000, **25**, 462.
9. G. Wider, *Prog. NMR Spectrosc.*, 1998, **32**, 193.
10. K. Pervushin, R. Riek, G. Wider, and K. Wüthrich, *Proc. Natl. Acad. Sci. USA*, 1997, **94**, 12 366.
11. K. Pervushin, G. Wider, R. Riek, and K. Wüthrich, *Proc. Natl. Acad. Sci. USA*, 1999, **96**, 9607.
12. K. Pervushin, G. Wider, and K. Wüthrich, *J. Biomol. NMR*, 1998, **12**, 345.
13. G. Bodenhausen and D. J. Ruben, *Chem. Phys. Lett.*, 1980, **69**, 185.
14. K. Pervushin, R. Riek, G. Wider, and K. Wüthrich, *J. Am. Chem. Soc.*, 1998, **120**, 6394.
15. K. Wüthrich, 'NMR of Proteins and Nucleic Acids', Wiley: New York, 1986.
16. S. B. Shuker, P. J. Hajduk, R. P. Meadows, and S. W. Fesik, *Science*, 1996, **274**, 1531.
17. M. Pellecchia, P. Sebbel, U. Hermanns, K. Wüthrich, and R. Glockshuber, *Nature Struct. Biol.*, 1999, **6**, 336.
18. B. Brutscher, J. Boisbouvier, A. Pardi, D. Marion, and J. P. Simorre, *J. Am. Chem. Soc.*, 1998, **120**, 11 845.
19. R. Fiala, J. Czernek, and V. Sklenár, *J. Biomol. NMR*, 2000, **16**, 291.
20. G. A. Jeffrey and W. Saenger, 'Hydrogen Bonding in Biological Structures', Springer: Berlin, 1991.
21. A. J. Dingley and S. Grzesiek, *J. Am. Chem. Soc.*, 1998, **120**, 8293.
22. K. Pervushin, A. Ono, C. Fernandéz, T. Szyperski, M. Kainosho, and K. Wüthrich, *Proc. Natl. Acad. Sci. USA*, 1998, **95**, 14 147.
23. F. Cordier and S. Grzesiek, *J. Am. Chem. Soc.*, 1999, **121**, 1601.
24. Y. X. Wang, J. Jacob, F. Cordier, P. Wingfield, S. J. Stahl, S. Lee-Huang, D. Torchia, S. Grzesiek, and A. Bax, *J. Biomol. NMR*, 1999, **14**, 181.
25. L. E. Kay and K. H. Gardner, *Curr. Opin. Struct. Biol.*, 1997, **7**, 722.
26. M. Salzmann, G. Wider, K. Pervushin, H. Senn, and K. Wüthrich, *J. Am. Chem. Soc.*, 1999, **121**, 844.
27. A. Bax and S. Grzesiek, *Acc. Chem. Res.*, 1993, **26**, 131.
28. M. Salzmann, K. Pervushin, G. Wider, H. Senn, and K. Wüthrich, *J. Am. Chem. Soc.*, 2000, **122**, 7543.
29. M. Salzmann, K. Pervushin, G. Wider, H. Senn, and K. Wüthrich, *J. Biomol. NMR*, 1999, **14**, 85.
30. T. Yamazaki, T. Otomo, N. Oda, K. Kyogoku, K. Uegaki, N. Ito, Y. Ishino, and H. Nakamura, *J. Am. Chem. Soc.*, 1998, **120**, 5591.
31. T. W. Muir, D. Sondhi, and P. A. Cole, *Proc. Natl. Acad. Sci. USA*, 1998, **95**, 6705.
32. T. Otomo, K. Teruya, K. Uegaki, T. Yamazaki, and Y. Kyogoku, *J. Biol. NMR*, 1999, **14**, 105.
33. R. Xu, B. Ayers, D. Cowburn, and T. W. Muir, *Proc. Natl. Acad. Sci. USA*, 1999, **96**, 388.
34. G. A. Morris and R. Freeman, *J. Am. Chem. Soc.*, 1979, **101**, 760.
35. R. Riek, G. Wider, K. Pervushin, and K. Wüthrich, *Proc. Natl. Acad. Sci. USA*, 1999, **96**, 4918.
36. M. Goldman, *J. Magn. Reson.*, 1984, **60**, 437.
37. H. Takahashi, T. Nakanishi, K. Kami, Y. Arata, and I. Shimada, *Nature Struct. Biol.*, 2000, **7**, 220.
38. M. Pellecchia, D. S. Sim, and K. Wüthrich, *Nature Rev. Drug Disc.*, 2002, **4**, 211.
39. G. Zhu, X. M. Kong, and K. H. Sze, *J. Biomol. NMR*, 1999, **13**, 77.
40. A. Meissner and O. W. Sørensen, *J. Magn. Reson.*, 2000, **142**, 195.
41. C. Fernandéz, K. Adeishvili, and K. Wüthrich, *Proc. Natl. Acad. Sci. USA*, 2001, **98**, 2358.
42. C. Fernandéz, C. Hilty, S. Bonjour, K. Adeishvili, K. Pervushin, and K. Wüthrich, *FEBS Lett.*, 2001, **504**, 173.
43. A. Arora, F. Abildgaard, J. H. Bushweller, and L. Tamm, *Nature Struct. Biol.*, 2001, **8**, 334.
44. C. Hennig, A. Arcy, I. Hampele, M. G. P. Page, C. Oefner, and G. E. Dale, *Nature Struct. Biol.*, 1998, **5**, 357.
45. M. Salzmann, G. Wider, K. Pervushin, and K. Wüthrich, *J. Biomol. NMR*, 1999, **15**, 181.
46. M. Salzmann, K. Pervushin, G. Wider, H. Senn, and K. Wüthrich, *Proc. Natl. Acad. Sci. USA*, 1998, **95**, 13 585.

Acknowledgements

Financial support was obtained from the Schweizerischer Nationalfonds (Project 31.49047.96).

Copyright © 2003 John Wiley & Sons, Ltd.